Electronic Supplementary Material (ESI) for Materials Advances.

Electronic Supplementary Information for:

Controlling the Dispersion of Ceria Using Nanoconfinement: Application to CeO_2/SBA-15 Catalysts for NH_3-SCR

Jun Shen and Christian Hess*

Eduard-Zintl-Institut für Anorganische und Physikalische Chemie, Technical University of Darmstadt, Alarich-Weiss-Str. 8, 64287 Darmstadt, Germany. Email: jun.shen@tu-darmstadt.de; christian.hess@tu-darmstadt.de

Figure S1 Schematic diagrams of pore shapes of the three tested samples.

(a)

(i) Water-acid azeotrope formation:

$$Ce(NO_3)_3 \cdot 6H_2O \rightarrow Ce(OH)_b(NO_3)_{3-b}(H_2O)_{6-b-c} + b\ HNO_3 + c\ H_2O$$

(ii) NO_3^- thermal decomposition:

$$4\ Ce(NO_3)_3 \cdot 6H_2O \rightarrow 4\ Ce(OH)_3 + 12\ NO_x + (15-6x)\ O_2 + 18\ H_2O$$

(iii) Cerium hydroxide condensation:

$$Ce(OH)_4 \rightarrow CeO_2 + 2H_2O$$

(b)

(i) Dehydration:

$$Ce(NO_3)_3 \cdot 6H_2O \rightarrow Ce(NO_3)_3 + 6\ H_2O$$

(ii) Decomposition to CeO_2:

$$Ce(NO_3)_3 \rightarrow Ce(NO_3)_2 + NO_2 + ½\ O_2$$

$$Ce(NO_3)_2 \rightarrow CeNO_3 + NO_2 + ½\ O_2$$

$$CeNO_3 \rightarrow CeO_2 + NO$$

Figure S2 According to Cochran et al.((a)),[1] the weight loss can be subdivided into three stages: (i) prior to decomposition, the salt melts and releases loosely bound water (<100 °C), or evaporates as aqueous acid azeotrope at a boiling point of about 120 °C; (ii) at higher temperature (>266 °C), residual nitrate thermally decomposes into NO_x gas and forms a solid metal hydroxide product; (iii) the resulting cerium hydroxide condenses to form ceria. Kang et al. have proposed a more detailed mechanism for the decomposition of $Ce(NO_3)_3$ ((b)) according to which $Ce(NO_3)_3$ transforms first to $Ce(NO_3)_2$ at about 245 °C, then to $Ce(NO_3)$ at about 270 °C, and finally to CeO_2 at about 295 °C.[2]

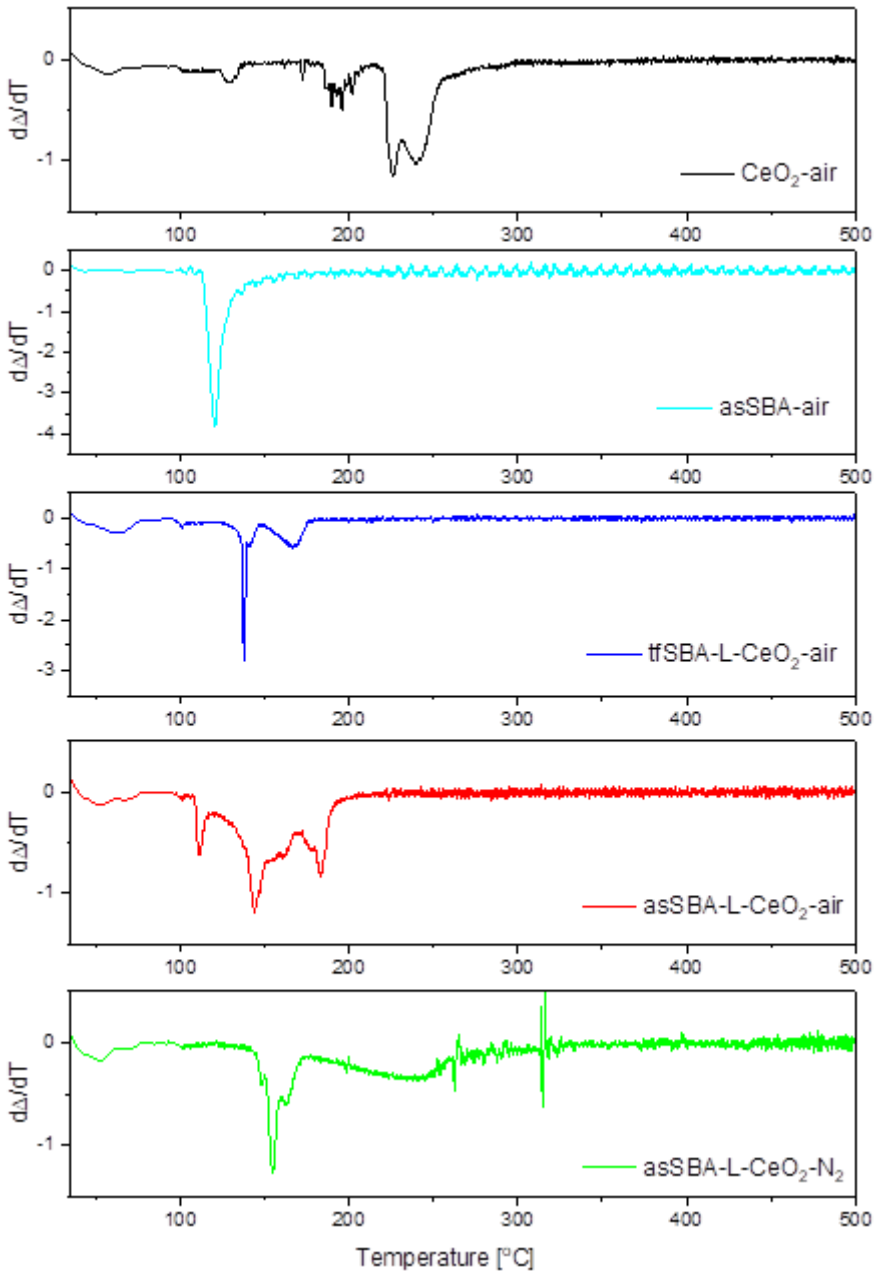

Figure S3 DTG profiles of pure cerium nitrate, asSBA-15, and mixtures of SBA-15 and cerium nitrate during heating to 500 °C in air or inert N_2 (heating rate: 1.5 °C/min).

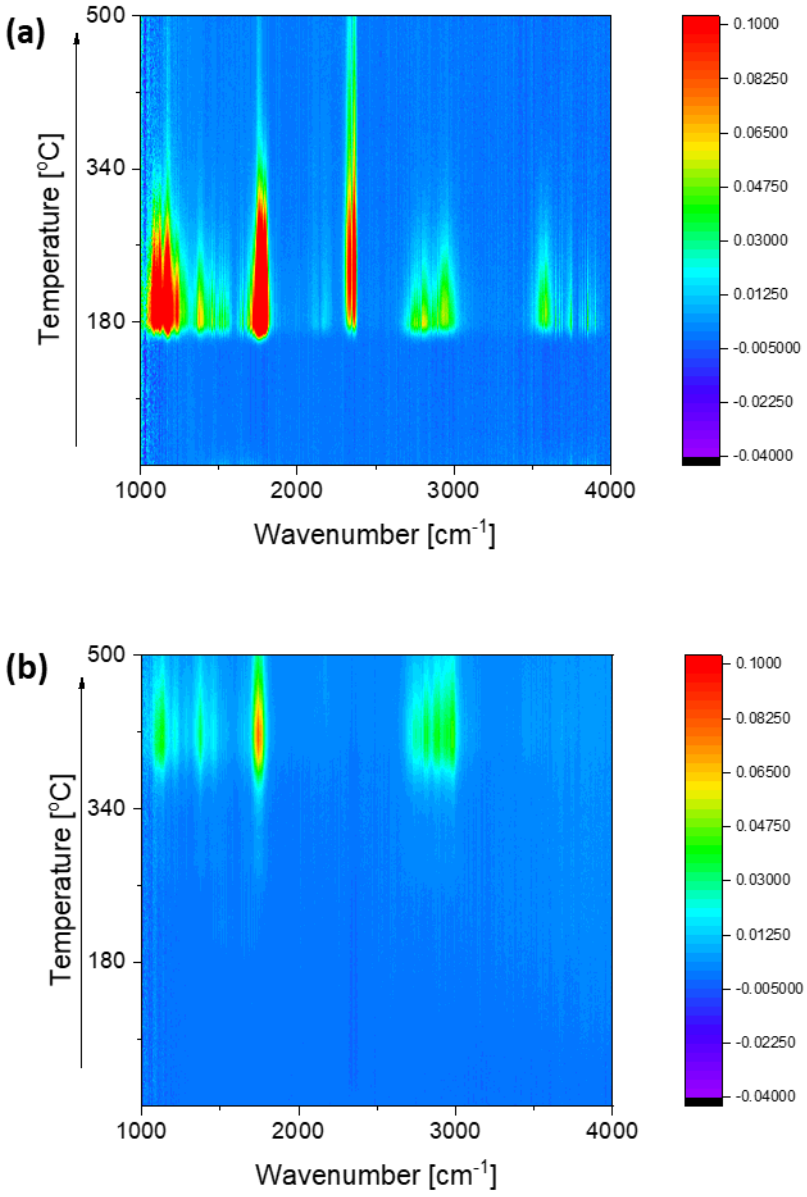

Figure S4 *In situ* detection of exhaust during calcination of samples (a) asSBA15-air, (b) asSBA15-N_2.

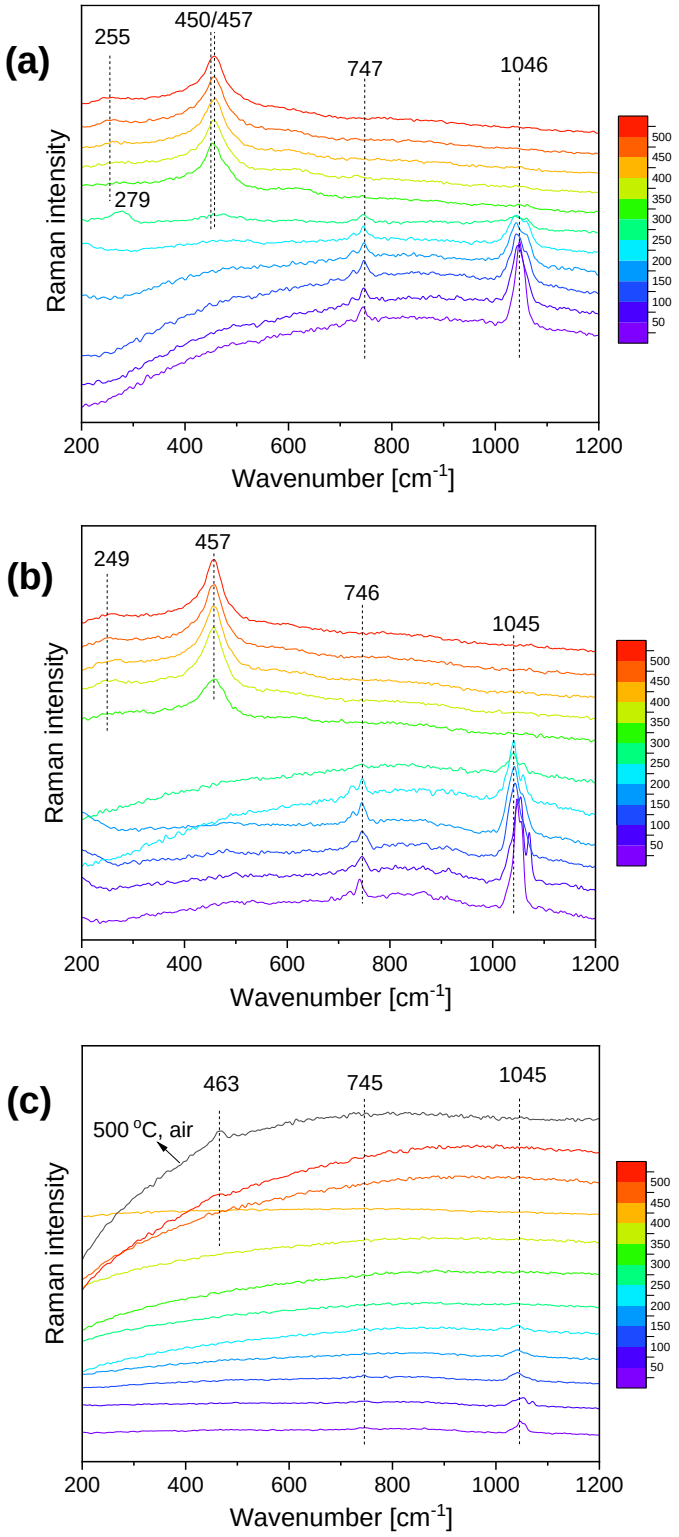

Figure S5 *In situ* Raman spectra (514.5 nm) during the calcination of (a) tfSBA-L-CeO_2-air, (b) asSBA-L-CeO_2-air, and (c) asSBA-L-CeO_2-N_2, following the protocol given in Fig. 1a. Spectra are offset for clarity. The feature at about 250 cm^{-1} has been shown to originate from the longitudinal stretching mode of surface oxygen against cerium ions (Ce-O) as well as a contribution of the 2TA phonon,[3,4] whereas the additional feature at about 279 cm^{-1} is tentatively assigned to a nitro species formed during the transformation from cerium nitrate to crystalline ceria.[5]

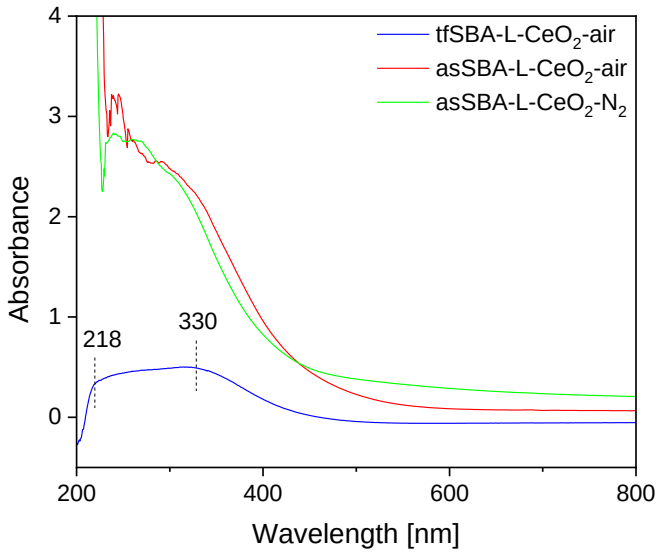

Figure S6 DR UV-vis spectra of the samples tfSBA-L-CeO_2-air, asSBA-L-CeO_2-air, and asSBA-L-CeO_2-N_2, recorded at room temperature after cooling from high temperature calcination in synthetic air.

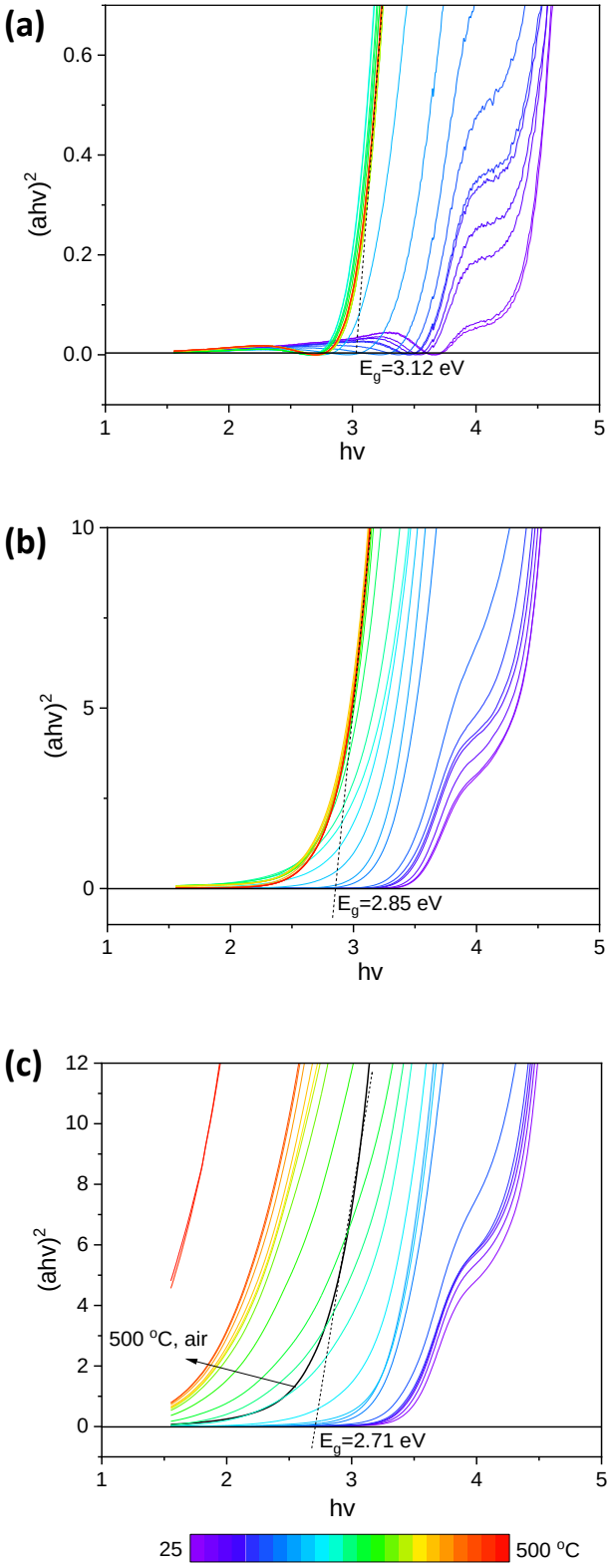

Figure S7 Calculation of band gap energies according to the *in situ* DR UV-vis spectra by applying Tauc's method. (a) tfSBA-L-CeO_2-air, (b) asSBA-L-CeO_2-air, and (c) asSBA-L-CeO_2-N_2. In (c) the black curve represents the sample calcined in N_2, followed by calcination in air at 500 °C for 2 hours.

Table S1 Assignment of the IR features observed by *in situ* DRIFT spectroscopy.

Wavenumber, cm^{-1}	tfSBA-CeO_2-air	asSBA-CeO_2-air	asSBA-CeO_2-N_2	Ref.
1225-1237		Hydrogen carbonates	Hydrogen carbonates	6
1253	Chelate NO_2^-			7
1303	Monodentate nitrates			8
1345-1357	Free nitrate ions		Free nitrate ions	8
1458			C-H deformation	9
1539-1543	Bidentate nitrates	Bidentate nitrates		10
1613	Bridging nitrates			10
1625-1636	Adsorbed NO_2	Adsorbed NO_2	Adsorbed NO_2	8
1663	Adsorbed N_2O_4			8
1729-1732		C=O	C=O	7
1764-1767	Adsorbed NO	Adsorbed NO	Adsorbed NO	7
1849-1981	Silica framework	Silica framework	Silica framework	8
2290/2341		Adsorbed CO_2		7
2356-2360	CO_2	CO_2	CO_2	11
2484-2491	C-H	C-H	C-H	12
2809	C-H_2			13
2867/2933/2976		C-H	C-H	11
2941	CH_2			9
3176	-OH			14
3266	-OH			13
3200-3500	-OH			13
3700			Ce-OH	15
3740	Si-OH	Si-OH		13

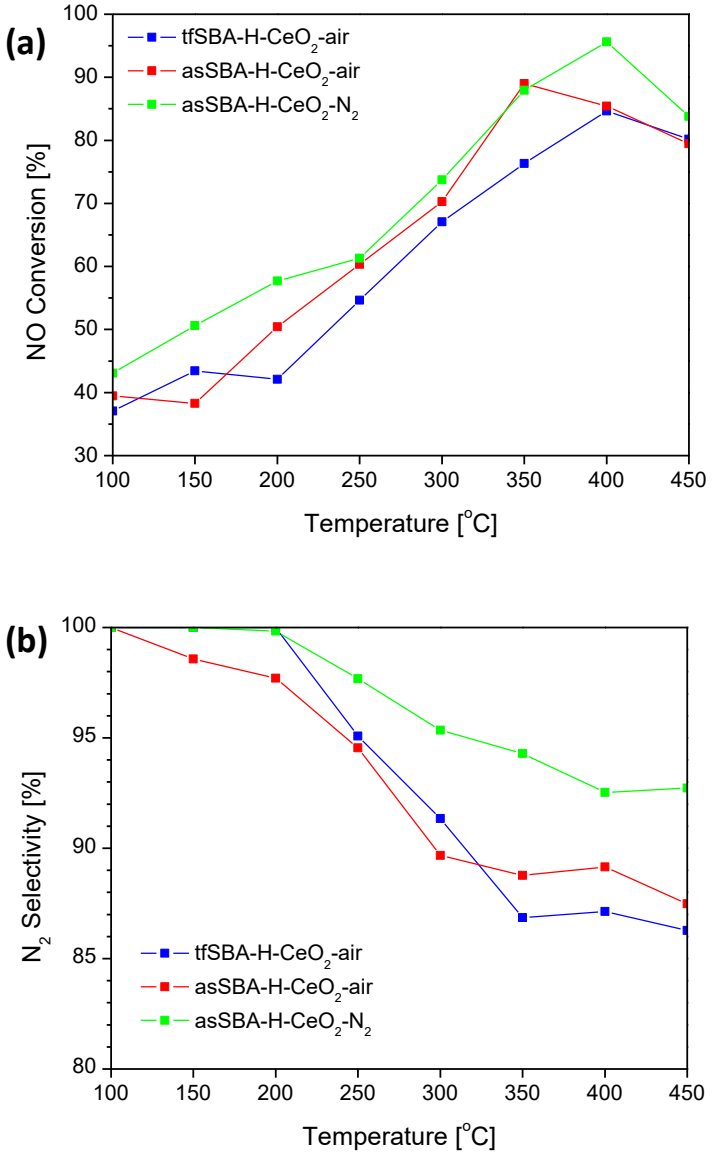

Figure S8 (a) NO conversion and (b) N_2 selectivity of the indicated samples in NH_3-SCR of NO, using a feed gas consisting of 500 ppm NH_3, 500 ppm NO, and 5% O_2 (balanced with N_2) and a total gas flow of 50 ml·min^{-1} (GHSV=30000 h^{-1}).

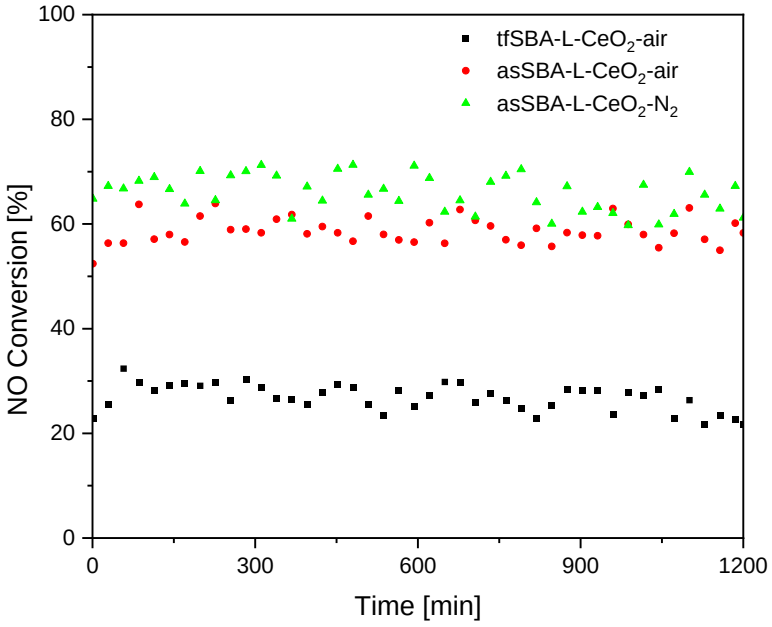

Figure S9 Stability of the indicated samples in NH_3-SCR of NO at 300 °C, using a feed gas consisting of 500 ppm NH_3, 500 ppm NO, and 5% O_2 (balanced with N_2) and a total gas flow of 50 ml·min^{-1} (GHSV=30000 h^{-1}).

Table S2 Catalytic performance of cerium-based deNO_x catalysts synthesized by different methods.

Catalyst	Preparation method	Reaction conditions	NO_x conversion (temperature range)	GHSV or GWSV	Source
CeO_2	precipitation method	NO = 600 ppm, NH_3 = 600, ppm, O_2 = 5%	45-60% (225-350 °C）	108000 h^{-1}	[16]
CeO_2	hydrothermal method	NH_3 = NO = 500 ppm, O_2 = 3%	50% (300 °C)	120000 ml g^{-1} h^{-1}	[17]
CeO_2	thermal decomposition	NO = 736 mg/m^3, NH_3 = 417 mg/m^3, O_2 = 5%	60-65% (300-400 °C)	108000 h^{-1}	[18]
CeO_2	impregnation	NH_3 = NO = 500 ppm, O_2 = 5%	15-20 % (350-450 °C)	120000 ml $g^{-1}h^{-1}$	[19]
CeO_2	thermal decomposition	NH_3 = NO = 600 ppm, O_2 = 5%	40-50% (250-325 °C)	108000 h^{-1}	[20]
CeO_2	one-pot	NH_3 = NO = 500 ppm, O_2 = 3%	50-60% (300-400 °C)	45000 h^{-1}	[21]
CeO_2	spread self-combustion	NH_3 = NO = 500 ppm, O_2 = 5%	15 % (300-500 °C)	200000 ml $g^{-1}h^{-1}$	[22]
CeO_2/SiO_2	wet impregnation	NH_3 = NO = 500 ppm, O_2 = 5%	70-80% (275-325 °C)	48000 ml $g^{-1}h^{-1}$	[23]
CeO_2/SBA-15	wet impregnation	NH_3 = 1100 ppm, NO = 1000 ppm, O_2 = 5%	60-70% (200-300 °C)	10000 h^{-1}	[24]
tfSBA-CeO_2-air	solid-state impregnation	NH_3 = NO = 500 ppm, O_2 = 5%	30% (300-400 °C)	30000 h^{-1} (150000 ml $g^{-1}h^{-1}$)	This work
asSBA-CeO_2-air	solid-state impregnation	NH_3 = NO = 500 ppm, O_2 = 5%	50-60% (250-400 °C)	30000 h^{-1} (150000 ml $g^{-1}h^{-1}$)	This work
asSBA-CeO_2-N_2	solid-state impregnation	NH_3 = NO = 500 ppm, O_2 = 5%	55-65% (200-450 °C)	30000 h^{-1} (150000 ml $g^{-1}h^{-1}$)	This work

References

1 E. A. Cochran, K. N. Woods, D. W. Johnson, C. J. Page and S. W. Boettcher, *J. Mater. Chem. A*, 2019, **7**, 24124-24149.

2 W. Kang, D. O. Ozgur and A. Varma, *ACS Appl. Nano Mater.*, 2018, **1**, 675-685.

3 C. Schilling, A. Hofmann, C. Hess and M. V. Ganduglia-Pirovano, *J. Phys. Chem. C*, 2017, **121**, 20834-20849.

4 A. Filtschew, D. Stranz and C. Hess, *Phys. Chem. Chem. Phys.*, 2013, **15**, 9066-9069.

5 C. Hess and J. H. Lunsford, *J. Phys. Chem. B*, 2002, **106**, 6358-6360.

6 S. M. Lee, Y. H. Lee, D. H. Moon, J. Y. Ahn, D. D. Nguyen, S. W. Chang and S. S. Kim, *Ind. Eng. Chem. Res.*, 2019, **58**, 8656-8662.

7 L. Y. Wang, Z. Q. Wang, X. X. Cheng, M. Z. Zhang, Y. K. Qin and C. Y. Ma, *RSC Adv.*, 2017, **7**, 7695-7710.

8 R. Wu, N. Q. Zhang, L. C. Li, H. He, L. Y. Song and W. G. Qiu, *Catalysts*, 2018, **8**.

9 D. Parimi, V. Sundararajan, O. Sadak, S. Gunasekaran, S. S. Mohideen and A. Sundaramurthy, *ACS Omega*, 2019, **4**, 104-113.

10 C. X. Wang, D. Z. Ren, J. C. Du, Q. G. Qin, A. M. Zhang, L. Chen, H. Cui, J. L. Chen and Y. K. Zhao, *Catalysts*, 2020, **10**.

11 H. Song, B. Mirkelamoglu and U. S. Ozkan, *Appl. Catal. A*, 2010, **382**, 58-64.

12 N. Bourenane, Y. Hamlaoui, C. Remazeilles and F. Pedraza, *Materials and Corrosion-Werkstoffe Und Korrosion*, 2019, **70**, 110-119.

13 C. Vittoni, G. Gatti, G. Paul, E. Mangano, S. Brandani, C. Bisio and L. Marchese, *ChemistryOpen*, 2019, **8**, 719-727.

14 B. Xu, Y. W. Liu, Y. Li, L. L. Wang, N. N. Li, M. Fu, P. Wang and Q. Wang, *New. J. Chem.*, 2018, **42**, 11796-11803.

15 Z. L. Wu, Y. Q. Cheng, F. Tao, L. Daemen, G. S. Foo, L. Nguyen, X. Y. Zhang, A. Beste and A. J. Ramirez-Cuesta, *J. Am. Chem. Soc.*, 2017, **139**, 9721-9727.

16 F. D. Liu, W. P. Shan, X. Y. Shi, C. B. Zhang and H. He, *Chin. J. Catal.*, 2011, **32**, 1113-1128.

17 X. L. Hu, J. X. Chen, W. Y. Qu, R. Liu, D. R. Xu, Z. Ma and X. F. Tang, *Environ. Sci. Technol.*, 2021, **55**, 5435-5441. 2018, **353**, 930-939.

18 H. Lv, X. Hua, W. Xie, Q. Hu, J. Wu and R. Guo, *J. Rare Earths*, 2018, **36**, 708-714.

19 H. L. Zhang, L. Ding, H. M. Long, J. X. Li, W. Tan, J. W. Ji, J. F. Sun, C. J. Tang and L. Dong, *J. Rare Earths*, 2020, **38**, 883-890.

20 X. Sun, R.-T. Guo, S.-W. Liu, J. Liu, W.-G. Pan, X. Shi, H. Qin, Z.-Y. Wang, Z.-Z. Qiu and X.-Y. Liu, *Appl. Surf. Sci.*, 2018, **462**, 187-193.

21 Y. Q. Zeng, Y. N. Wang, S. L. Zhang, Q. Zhong, W. L. Rong and X. H. Li, *J. Colloid Interface Sci.*, 2018, **524**, 8-15.

22 Z.-B. Xiong, Z.-Z. Li, C.-X. Li, W. Wang, W. Lu, Y.-P. Du and S.-l. Tian, *Appl. Surf. Sci.*, 2021, **536**, 147719.

23 W. Tan, A. N. Liu, S. H. Xie, Y. Yan, T. E. Shaw, Y. Pu, K. Guo, L. L. Li, S. H. Yu, F. Gao, F. D. Liu and L. Dong, *Environ. Sci. Technol.*, 2021, **55**, 4017-4026.

24 X. Q. Ran, M. H. Li, K. Wang, X. Y. Qian, J. W. Fan, Y. Sun, W. Luo, W. Teng, W. X. Zhang and J. P. Yang, *ACS Appl. Mater. Interfaces*, 2019, **11**, 19242-19251.